$CaCO_3$ Biomineralization: Acidic 8-kDa Proteins Isolated from Aragonitic Abalone Shell Nacre Can Specifically Modify Calcite Crystal Morphology

Germaine Fu,[†] Suresh Valiyaveettil,[‡] Brigitte Wopenka,[§] and Daniel E. Morse*[,†,||]

Biomolecular Science and Engineering Graduate Program and the Institute for Collaborative Biotechnologies, University of California at Santa Barbara, Santa Barbara, California 93106, Department of Chemistry, National University of Singapore, Singapore 117543, and the Department of Earth and Planetary Sciences, Washington University, St. Louis, Missouri 63130

Received October 30, 2004; Revised Manuscript Received January 11, 2005

Acidic proteins from many biogenic minerals are implicated in directing the formation of crystal polymorphs and morphologies. We characterize the first extremely acidic proteins purified from biomineralized aragonite. These abalone nacre proteins are two variants of 8.7 and 7.8 kDa designated AP8 (for aragonite proteins of approximately 8 kDa). The AP8 proteins have compositions dominated by Asx (∼35 mol %) and Gly (∼40 mol %) residues, suggesting that their structures have high Ca^{2+}-binding capacity and backbone flexibility. The growth of asymmetrically rounded $CaCO_3$ crystals in the presence of AP8 reveals that both proteins preferentially interact with specific locations on the crystal surface. In contrast, $CaCO_3$ crystals grown with nacre proteins depleted of AP8 retain the morphology of unmodified calcite rhombohedra. Our observations thus identify sites of protein−mineral interaction and provide evidence to support the long-standing theory that acidic proteins are more effective crystal-modulators than other proteins from the same biomineralized material.

Introduction

Biominerals are composites of inorganic minerals (such as calcite, aragonite, or hydroxylapatite) and organic macromolecules (such as proteins, polysaccharides, and proteoglycans) that serve the diverse functions of protection, skeletal support, and sensory detection.[1] These specialized structures, which include among others seashells, coccoliths, bones, teeth, otoliths, and magnetosomes, are the product of cooperative interactions between biomolecules and mineral-forming ions secreted into a membrane-delineated or extracellular space.[2] The resulting biogenic minerals typically differ from geological or synthetic inorganic minerals in crystal size, shape, orientation, and crystalline structure (also called "polymorph"), apparently defying the requirements of symmetry and thermodynamic stability inherent to the crystal lattice. Furthermore, many biominerals are organized from the nano- to macroscopic scales to form structures with hierarchical long-range order. The shell of the red abalone is a biomineralized structure that displays all these features. This mollusk shell contains an outer layer of calcite crystals and an inner layer of nacre that is formed from aragonite crystals. While calcite and aragonite are both chemically $CaCO_3$, their distinct atomic lattice organizations define them as separate polymorphs. Calcite is the most stable polymorph under ambient conditions of atmospheric pressure and moderate temperature. Thus, the abalone exoskeleton is composed of both the most stable crystalline polymorph (calcite) and a less stable polymorph (aragonite) of $CaCO_3$. Multiple complex microstructures are formed from these crystals in spatially distinct regions of the shell: bundles of prismatic calcite crystals make up the outer layer and stacks of aragonite tablets constitute nacre.[3−6] The combination of features presented by the shell, including (1) crystal sizes, shapes, and distribution; (2) two spatially separated mineral polymorphs; and (3) its organization as an organic/inorganic composite, may reflect adaptations that enhance the mechanical strength of the shell, which has a measured value that is higher than mineral alone.[7] Materials synthesized to mimic the ultrastructure of this biomineral composite[8,9] have not reproduced the precision of crystal formation achieved by the organism under the mild conditions of environmental temperature, pressure, and pH, due to incomplete knowledge of the molecules involved in controlling $CaCO_3$ biomineralization. While only present in small amounts, the organic components of mollusk shells determine the nucleation and stabilization of crystals with defined shapes and polymorphs under ambient conditions. This control is thought to result, in part, from templating crystal nucleation and from growth-modulating interactions with crystal surfaces. Thus, investigating the interactions between specific molecules, such as proteins, and the crystals whose growth they control is an important step toward understanding, and possibly mimicking, the complex process of $CaCO_3$ biomineralization.

* To whom correspondence should be addressed. Tel: 805-893-8982. Fax: 805-893-8062. E-mail: d_morse@lifesci.ucsb.edu.

[†] Biomolecular Science and Engineering Graduate Program, University of California at Santa Barbara.

[‡] National University of Singapore.

[§] Washington University.

[||] Institute for Collaborative Biotechnologies, University of California at Santa Barbara.

10.1021/bm049314v CCC: $30.25 © 2005 American Chemical Society
Published on Web 03/09/2005

The ubiquitous detection of acidic proteins within various calcareous biominerals has led to the prevalent speculation that these macromolecules, through interactions with positively charged calcium ions in solution or at the mineral surface, are the most influential during mineral formation.[10−12] Attempts to experimentally validate this hypothesis have been hindered, however, by limited quantities of anionic protein species purified in their mature form from biogenic minerals. Although the advent of cDNA library construction from molluskan tissue has yielded the primary sequences of several shell proteins,[13−17] exceptionally acidic proteins have proven resilient to conventional biochemical analyses. While a few sequences corresponding to highly acidic proteins from the calcitic layer of mollusk shells have been recently described,[18,19] the effects of these proteins on crystal growth remain unknown. Crystal growth studies with acidic protein mixtures and protein fractions isolated from invertebrate biominerals suggest that these proteins function to stabilize amorphous calcium carbonate,[20,21] nucleate crystalline phases,[22,23] template crystal orientation,[22] and modulate crystal morphology.[24−27] However, to ultimately assign specific roles to individual acidic proteins, they must first be effectively isolated from biomineralized composites.

We report the identification, purification, and partial characterization of two novel proteins from abalone shell nacre. Nacre-occluded proteins have received wide attention for their presumed role as determinants of the high-energy polymorph and morphology of the aragonite tablets that constitute nacre.[28] The proteins described here, designated AP8 for aragonite proteins of ca. 8 kDa, are the first ones selectively purified as the most acidic from biogenic aragonite and examined for their influence on $CaCO_3$ crystal growth.

Materials and Methods

Abbreviations. AP8, aragonite proteins of 8 kDa; MQ, MilliQ water; TFA, trifluoroacetic acid; SDS−PAGE, sodium dodecyl sulfate−polyacrylamide gel electrophoresis; Tricine, *N*-[2-hydroxyl-1,1-bis(hydroxymethyl)ethyl]glycine; HPLC, high-pressure liquid chromatography; MALDI-TOF, matrix-assisted laser desorption ionization time-of-flight; SEM, scanning electron microscopy; XRD, X-ray diffraction; ESI-MS/MS, electrospray ionization tandem mass spectrometry.

Protein Isolation from Abalone Nacre. Red abalone (*Haliotis rufescens*) specimens of uniform age and size (8−9 cm) were obtained from The Cultured Abalone, Inc. (Goleta, CA). The outer calcitic layer of the shell was removed by sandblasting. The remaining inner layer of nacre was ground to a fine powder and confirmed to contain only aragonite by X-ray diffraction.[13,22] Aragonite powder was demineralized with 5% acetic acid at 4 °C for 8 h. The demineralized mixture was centrifuged to separate the insoluble proteins that form the intercrystalline cross-linked matrix from the acetic acid-soluble mineral-associated proteins. The supernatant containing the soluble nacre proteins was dialyzed extensively against Tris-buffered MQ water at 4 °C. Protein samples were analyzed by electrophoresis on 16% Tricine gels (Invitrogen) and bands were visualized by Coomassie Brilliant Blue as previously described.[13] To identify acidic proteins, gels were washed with 50% 2-propanol and stained with 0.005% w/v Stains-All solution.

AP8 Protein Purification. The total mixture of soluble nacre proteins was resuspended in cold ammonium bicarbonate (15 mM, pH 8) and stirred at 4 °C while solid $(NH_4)_2SO_4$ (Aldrich) was slowly added to produce an 80% saturated solution. The solution was centrifuged to separate the precipitated proteins from the charged proteins that remained soluble (i.e. AP8). The ammonium sulfate supernatant and resuspended pellet were separately dialyzed extensively against MQ water. To resolve the AP8 protein variants by HPLC, the supernatant was resuspended in 0.1% trifluoroacetic acid (TFA) and injected onto a reverse phase column (PepMap Silica C-18, 4.6 × 150 mm) connected to a PerSeptive BioCAD System for perfusion chromatography. The proteins were eluted with a 0−50% gradient of 0.1% TFA/95% acetonitrile over 60 min at a flow rate of 1 mL/min. Fractions were collected at 1 mL/min.

MALDI-TOF Mass Spectrometry and Amino Acid Analysis. HPLC fractions containing AP8 protein were resuspended in MQ water and small aliquots were taken for mass spectrometry and amino acid analyses. AP8 protein fractions were analyzed in an α-cyano-4-hydroxycinnamic acid matrix at a final concentration between 5 and 25 pmol protein/μL. The sample spots were irradiated using a 6 MW N_2 laser (Laser Science, Inc.) of wavelength 337 nm. AP8 protein ions were accelerated with a 25 kV accelerating voltage and MALDI-TOF analyses were performed using a Voyager BioSpectrometry Workstation (PerSeptive Biosystems).

In preparation for amino acid analysis, protein samples were hydrolyzed under vacuum in 6 N HCl with 10% phenol heated at 110 °C for 24 h. The hydrolysis residue from each sample was resuspended in NaS (Amino Acid Sample Dilution Buffer, Beckman). Samples and amino acid standards (Sigma) were analyzed by ion exchange HPLC with ninhydrin-based detection on a Beckman System 6300 Auto Amino Acid Analyzer. The gradient program was that previously used to chromatographically separate phenylthiohydantoin derivatives of amino acids.[29]

In Vitro Crystal Growth Experiments. To prepare for use as the crystal growth substrate, Kevlar 29 fibers (Dupont) were partially hydrolyzed with 1.5 N NaOH as previously described to increase surface hydrophilicity and promote dense crystal nucleation.[30] All reagents and control proteins were purchased from Sigma. Small bundles of treated Kevlar fibers ~1 cm in length were placed in the bottom of wells in tissue culture plates (Falcon). The wells were filled with 12 mM $CaCl_2$ (pH 5.5−6) to cover the fibers. Nacre protein fractions resuspended in water were added to the wells at a final concentration of 10 μg/mL. Bovine serum albumin (BSA) and a crude mixture of calmodulin + S100 proteins purified from bovine brain were used as control proteins at the same concentration of 10 μg/mL. To induce the growth of aragonite crystals, poly(vinyl alcohol) (M_w = 70−100 kDa) was added to wells at a final concentration of 100 μg/mL. Once additives were included in the wells, the tissue

culture plates were kept sealed at room temperature for 1−7 days in a glass desiccator (Corning) containing a dish of solid $(NH_4)_2CO_3$.

X-ray Diffraction and Scanning Electron Microscopy. After crystal growth, Kevlar fibers were rinsed and dried completely at 37 °C. The pH of the $CaCl_2$ solutions after crystallization ranged from 9.8 to 9.9. The $CaCO_3$ crystal polymorphs of the bulk samples were determined on a Bruker D8 Advance X-ray diffractometer with Cu−Kα radiation at 40 kV, 30 mA in $\theta-\theta$ geometry. X-ray diffraction (XRD) data were collected from 0.0361°/s scans of 20−60° 2θ using an M. Braun position-sensitive detector. Diffraction peaks were indexed using Diffrac Plus Release 2000 Eva 6.0 evaluation software (Bruker Advanced X-ray Solutions). The identified XRD patterns corresponded to the following JCPDS references: 24 - 0027 (calcite) and 41 - 1475 (aragonite). After XRD analysis, the samples were either used for Raman analysis or sputter-coated with gold and imaged on a JEOL 6300F cold cathode field emission scanning electron microscope.

Raman Microprobe Spectroscopy. Before and during Raman analysis the $CaCO_3$ crystals and the Kevlar fibers were optically imaged in reflected visible light, and the exact positions for analyses were preselected and documented. Raman spectra were obtained with an integrated, fiber-optically coupled microscope−spectrometer−detector Raman microprobe system from Kaiser Optical. The instrument is configured with a frequency-doubled Nd:YAG laser that emits 532-nm visible light with maximum output of 100 mW, an f/1.8 holographic spectrograph, a 2048-channel CCD array detector, and a research-grade Leica polarized-light microscope. The spectrograph covers the spectral range from 150 to 4300 Δcm^{-1} with a spectral resolution of 2.5 cm^{-1}. Peak positions can be measured with ±0.5 cm^{-1} accuracy. The laser spot size is ~1 μm, and the laser power at the sample surface was chosen to be 10 mW. Data were collected with HoloGRAMS V. 4.0 data collection software, and processed with GRAMS32 software by Galactic.

Results

AP8 Protein Purification and Biochemical Characterization. Proteins considered to have been occluded or intimately associated with the mineral phase of nacre are those that remained soluble in dilute acetic acid after demineralization. While acetic acid treatment may induce protein hydrolysis, this method of demineralization has been successful for recovering intact the soluble shell proteins AP7 and AP24 from abalone nacre, since the gel electrophoretic mass of the native proteins corresponded well to the calculated protein masses based on cDNA sequences.[13] The total mixture of these solubilized nacre proteins contained several protein species that were separated in SDS−PAGE gels: seven bands were observed to stain intensely with Coomassie Brilliant Blue, and several additional bands stained faintly at higher molecular masses (Figure 1, lane 1). The previously characterized nacre proteins AP7 and AP24[13] can be identified as bands migrating at the corresponding molecular masses indicated. To isolate the most

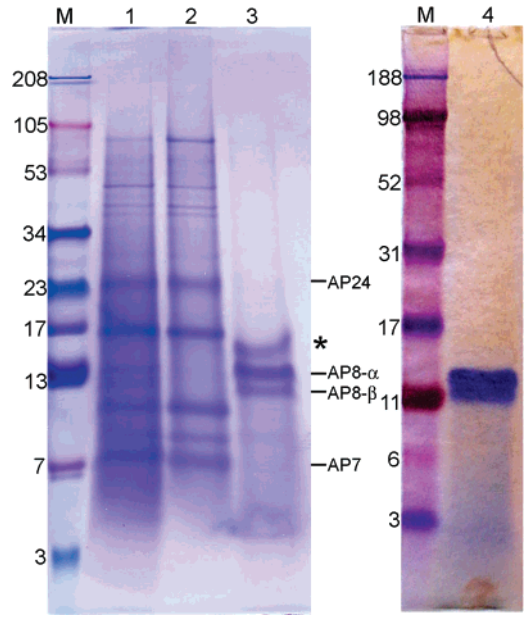

Figure 1. Gel electrophoresis of ammonium sulfate protein fractions: lane 1, total soluble nacre protein fraction after demineralization; lane 2, ammonium sulfate precipitate containing the majority of soluble nacre proteins including AP7 and AP24, except depleted for AP8; lane 3, ammonium sulfate supernatant containing AP8 proteins; the asterisk (*) labels the protein aggregate. The gel containing lanes 1−3 were stained with 0.3% Coomassie Brilliant Blue. Lane 4, AP8 proteins from the ammonium sulfate supernatant stained a deep blue color with Stains-All dye. Lanes labeled M contain markers with molecular masses indicated to the left.

acidic species of soluble nacre proteins, precipitation with ammonium sulfate was carried out to separate the more hydrophobic proteins from those that are more charged. Upon precipitation from an 80% saturated solution of $(NH_4)_2SO_4$, two distinct protein populations with virtually no overlap were visualized by gel electrophoresis. The majority of the soluble nacre proteins were precipitated in ammonium sulfate (Figure 1, lane 2). The retention of relative staining intensities indicated these protein populations were precipitated in their entirety. In contrast, the ammonium sulfate supernatant contained a protein doublet with apparent molecular masses of ca. 12 and 14 kDa (Figure 1, lane 3). Also seen in this fraction was a band consistent with a higher molecular mass aggregate likely formed by crowding at the high protein concentration (60−80 μg per lane; 1.0 mm thick gel) necessary for Coomassie visualization. The bands of the supernatant protein doublet were designated AP8-α and AP8-β for reasons discussed below (cf. Figure 3). Although clearly present in the initial mixture of solubilized nacre proteins (Figure 1, lane 1), the AP8 proteins were conspicuously absent from the ammonium sulfate pellet (Figure 1, lane 2). A lower concentration of the proteins from the ammonium sulfate supernatant (30 μg per lane; 1.0 mm thick gel) was visualized on a gel with Stains-All, a cationic carbocyanine dye that stains most proteins red, but stains Ca^{2+}-binding and other strongly anionic proteins blue.[31−33] Stains-All stained the AP8 proteins blue (Figure 1, lane 4), with staining intensity relatively higher than Coomassie Brilliant Blue (Figure 1, lane 3), demonstrating that the proteins are acidic and likely to bind Ca^{2+} ions.

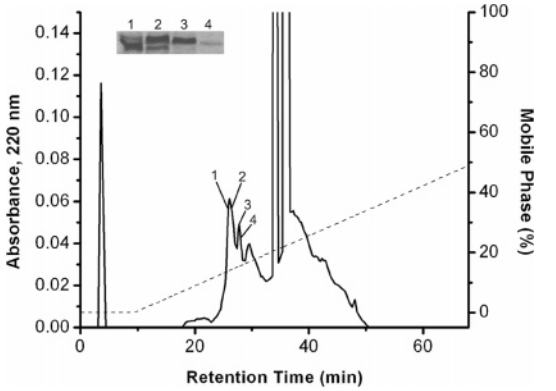

Figure 2. C-18 reverse phase HPLC purification of AP8 proteins. The ammonium sulfate supernatant protein fraction was loaded on a C-18 column. Elution was monitored by absorbance at 220 nm. The AP8 proteins eluted in four fractions of the two leading peaks, as visualized by SDS−PAGE with Coomassie staining (inset). The mobile phase (dashed line) is 95% acetonitrile/0.1% TFA. Even after extensive dialysis of the supernatant, a prominent salt peak was observed in the flow-through. No protein bands were observed in gels for fractions eluting from the two high absorbance peaks or from the broad peaks, indicating absorbance in these fractions was from nonprotein organic molecules such as pigments.

Although the AP8 proteins were the only ones observed in gels of the ammonium sulfate supernatant, the proteins were further purified for additional analyses and crystal growth experiments. Initial separation by ion exchange chromatography was not sufficient to either separate AP8 from other contaminating species, or to resolve the two AP8 variants from each other. In contrast, reverse-phase HPLC achieved both purification goals, in addition to eliminating the buffer salts that may interfere with crystal growth. The elution profile of the supernatant fractionated by HPLC on a C-18 column revealed multiple peaks (Figure 2). The AP8 proteins eluted in the leading peaks at 18−20% of the gradient, as visualized by electrophoresis (Figure 2, inset). The fractions containing the AP8 proteins reapplied to the column yielded only the same protein peaks upon rechromatography, indicating that the proteins were purified to homogeneity (data not shown). The elution order of HPLC fractions, which corresponded to the elution first of AP8-β, followed by the mixed population of AP8 proteins, and AP8-α last, indicated that AP8-α is slightly more hydrophobic than AP8-β (subsequently confirmed by amino acid analysis; cf. Table 1).

The HPLC-purified AP8 proteins observed on Coomassie-stained gels were analyzed by mass spectrometry to determine their exact masses (Figure 3). The protein of the AP8 doublet that migrated slower on the gel (Figure 3a, lane 3) corresponded to an 8.7 kDa species (Figure 3b), while the faster migrating protein on the gel (Figure 3a, lane 1) corresponded to a 7.8 kDa species (Figure 3c). The proteins were therefore designated AP8 for *a*ragonite *p*roteins of approximately *8* kDa. The labels α and β distinguish the two variants; AP8-α denotes the larger and more abundant protein. The exact masses of the proteins were calculated by positions of the $[M + H]^+$ and $[M + 2H]^{2+}$ peaks to be 8707.55 for AP8-α and 7839.64 for AP8-β. A considerable difference was observed between the protein masses determined by the two analytical methods. The apparent values indicated by gel electrophoresis are approximately 12 and 14 kDa (Figure 1, lane 3), while the true values revealed by mass spectrometry are approximately 8 kDa (Figure 3). This discrepancy suggests that the highly anionic AP8 proteins only bind weakly to SDS, causing their anomalous migration in gels that is dependent on charge densities as well as protein masses. This phenomenon has been previously reported for Glu-rich recombinant proteins.[34]

Table 1. Amino Acid Composition of AP8 Proteins and Nacre Protein Fractions with or without AP8

mol %	AP8-α (8.7 kDa)	AP8-β (7.8 kDa)	total nacre proteins	AP8-depleted nacre proteins
Asx	36.5	34.6	22.8	11.8
Thr	1.2	0.6	1.9	3.1
Ser	4.7	2.8	7.6	8.9
Glx	5.2	8.4	6.9	9.8
Pro	2.1	1.9	4.8	7.4
Gly	37.7	39.6	27.6	21.0
Ala	5.2	3.0	11.0	13.5
Val			2.0	3.0
Met			0.9	1.5
Ile			1.3	1.9
Leu			3.1	4.9
Tyr	0.4		1.5	2.4
Phe	1.2		2.3	2.4
His			0.6	1.0
Lys	2.8	4.7	1.8	2.4
Arg	3.0	4.3	4.0	4.4

Table 1 lists the amino acid compositions of the individual AP8 proteins as well as of total mixtures of soluble nacre proteins that do or do not contain AP8. As expected from their similar purification behaviors, the AP8 proteins also are similar in composition. Remarkably, nearly 75% of the compositions of the AP8 proteins are dominated by roughly equal proportions of Asx and Gly residues. Multiple Asp residues probably account for the anionic character of the AP8 proteins. However, since the Asx value includes Asp and Asn in indeterminate proportions, Asp in combination with modified Asn residues carrying terminal sialic acid or other anionic groups may be present in the AP8 sequences. Furthermore, while nonpolar residues excluding Gly only contribute approximately 6.7 mol % combined, about 17.7 mol % of the AP8 proteins are composed of the polar residues Lys, Arg, Ser, Thr, and Glx. These values indicate that the overall structures of the AP8 proteins are composed of charged and/or polar amino acids, as expected for proteins selected by solubility in 80% ammonium sulfate. The AP8 proteins are more extremely biased for Asx and Gly residues than the total protein fraction, although these two residues also contribute significantly to the composition of the total nacre protein fraction at roughly equal proportions (22.8 mol % Asx; 27.6 mol % Gly). In contrast, the Asx content in nacre proteins depleted of AP8 (11.8 mol %) has been reduced to nearly half of the Gly content (21.0 mol %), demonstrating that the majority of Asx residues in the total protein fraction are in AP8.

In Vitro Crystal Growth on Kevlar Fibers. The experimental design of crystal growth assays is based on previous studies of the biomimetic interaction between insoluble Kevlar fibers and the soluble polymer additive poly(vinyl

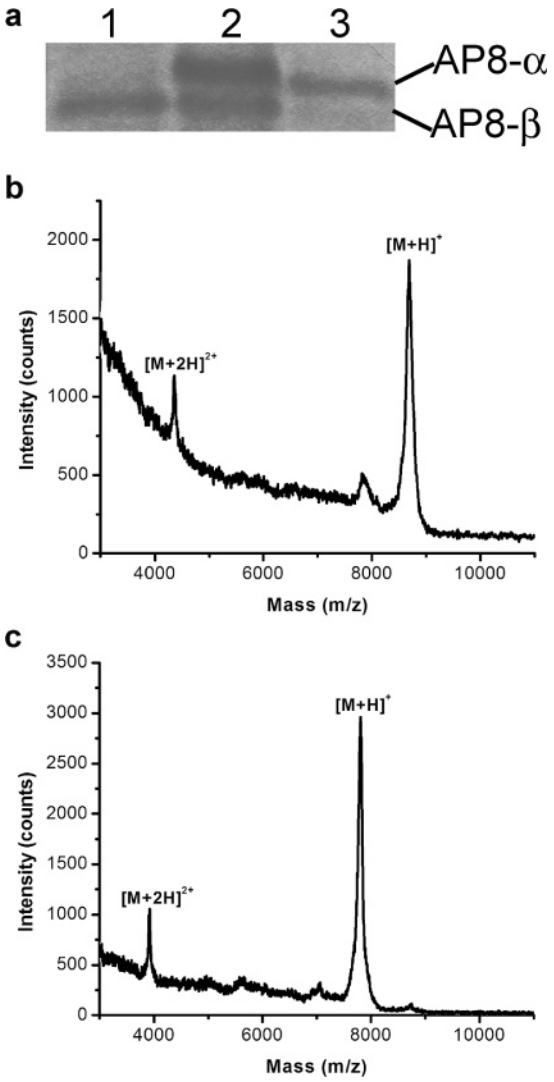

Figure 3. MALDI-TOF mass spectrometry of HPLC-purified AP8 proteins. (a) 16% Tricine gel electropherogram of AP8 proteins stained with Coomassie. Lane 1, AP8-β; lane 2, the AP8 protein doublet; lane 3, AP8-α. (b) Mass spectrum of AP8-α reveals mass of 8.7 kDa. (c) Mass spectrum of AP8-β reveals mass of 7.8 kDa.

alcohol) (PVA).[30] Kevlar fibers present a repetitive polyamide structure chemically identical to the polypeptide backbone of proteins, and, as a highly hydrophobic polymer, mimic the insoluble cross-linked matrix of proteins that surround crystals in the shell. $CaCO_3$ crystals were grown on Kevlar fibers in the presence or absence of various additives using the slow diffusion method, in which the rate of crystal formation is limited by dissolution of carbon dioxide generated by the sublimation of ammonium carbonate.[35,36] Under ambient conditions and in the absence of any additives, rhombohedral crystals of calcite, the most thermodynamically stable polymorph and shape of $CaCO_3$ at low temperatures, grew on the Kevlar fibers (data not shown). Furthermore, only calcite rhombohedra with very smooth surfaces were observed on the Kevlar fibers in the presence of control proteins (10 μg/mL of BSA or crude calmodulin) after 3 days of growth (Figure 4a). The polymorph was confirmed by the detection of calcite X-ray diffraction (XRD) peaks from the bulk sample (Figure 4b) and calcite Raman peaks from individual crystals (Figure 4d). The SEM (Figure 4a) and optical images (Figure 4c) verify that the crystals are the rhombohedral form of calcite expressing the symmetry-related {104} faces. The growth of unmodified smooth calcite rhombohedra in the presence of the acidic calcium-chelating calmodulin and S100 proteins validated the designation of these proteins as negative controls for nonspecific polyanion−mineral interactions.

Calcite Modification by Nacre Proteins. Calcium carbonate crystals were grown on Kevlar by slow diffusion in the presence of 10 μg/mL of nacre proteins for 1, 3, and 7 days. The total mixture of nacre proteins contained all the soluble aragonitic proteins, including AP8, AP7, and AP24, as visualized by gel electrophoresis (Figure 1, lane 1). After the first day of growth, slightly roughened calcite rhombs were observed (Figure 5a). The crystals reached their most modified state after 3 days of growth, when defined macrostepping at crystal edges and pitting at crystal faces were observed (Figure 5b). The emergence of macrosteps—differences in elevation at the crystal edges clearly visible at the micrometer-scale resolution of the SEM—was attributed to the bunching of elementary steps to produce larger (i.e. macro) steps. Neither the macrosteps nor the pitted faces were observed for comparable crystals grown in the presence of control proteins (Figure 4). With further growth in the presence of nacre proteins, the crystals appeared after 7 days as imperfect calcite rhombohedra still showing the effects of protein-induced modulation, as they were riddled with defects such as fissures at the crystal faces and edges (Figure 5c).

Comparative analyses of crystals grown in the presence of proteins precipitated by ammonium sulfate, and thus depleted of the AP8 proteins, were conducted. In contrast to the significantly modified crystal morphologies observed for the total mixture of proteins, the AP8-depleted collection of nacre proteins produced only slightly roughened calcite rhombohedra at all time points (Figure 5d−f). This observation indicated that the ability to modify calcite morphology by nacre proteins was dependent on the presence of the most acidic proteins, i.e., the AP8 proteins.

AP8-α and -β were isolated from each other by HPLC and incubated separately in the crystal growth assay. Since the same effects were seen for both of the AP8 proteins, representative images of crystals grown with either of the variants are shown (Figure 5g−i). After 1 day of incubation with AP8, rhombohedral crystals of calcite were observed with roughening along the edges between the {104} faces (Figure 5g). The most extremely affected crystals were observed after 3 days of growth with AP8 protein (Figure 5h). Under these conditions, the individual crystals were elongated with distinct macrostepping. Day 1 images in which the {104} faces of the crystals remained intact suggested that these macrosteps resulted from increased roughening at the edges of the rhombohedral faces. Moreover, most crystals grown in the presence of AP8 showed that two edges of each (104) face remained straight, while the other two edges became rounded. The resulting crystals therefore exhibited asymmetrically biased stepping only between the rounded edges. After 7 days of growth the crystals appeared to have a more rhombic shape than crystals grown for 3 days (Figure 5i), suggesting that the depletion

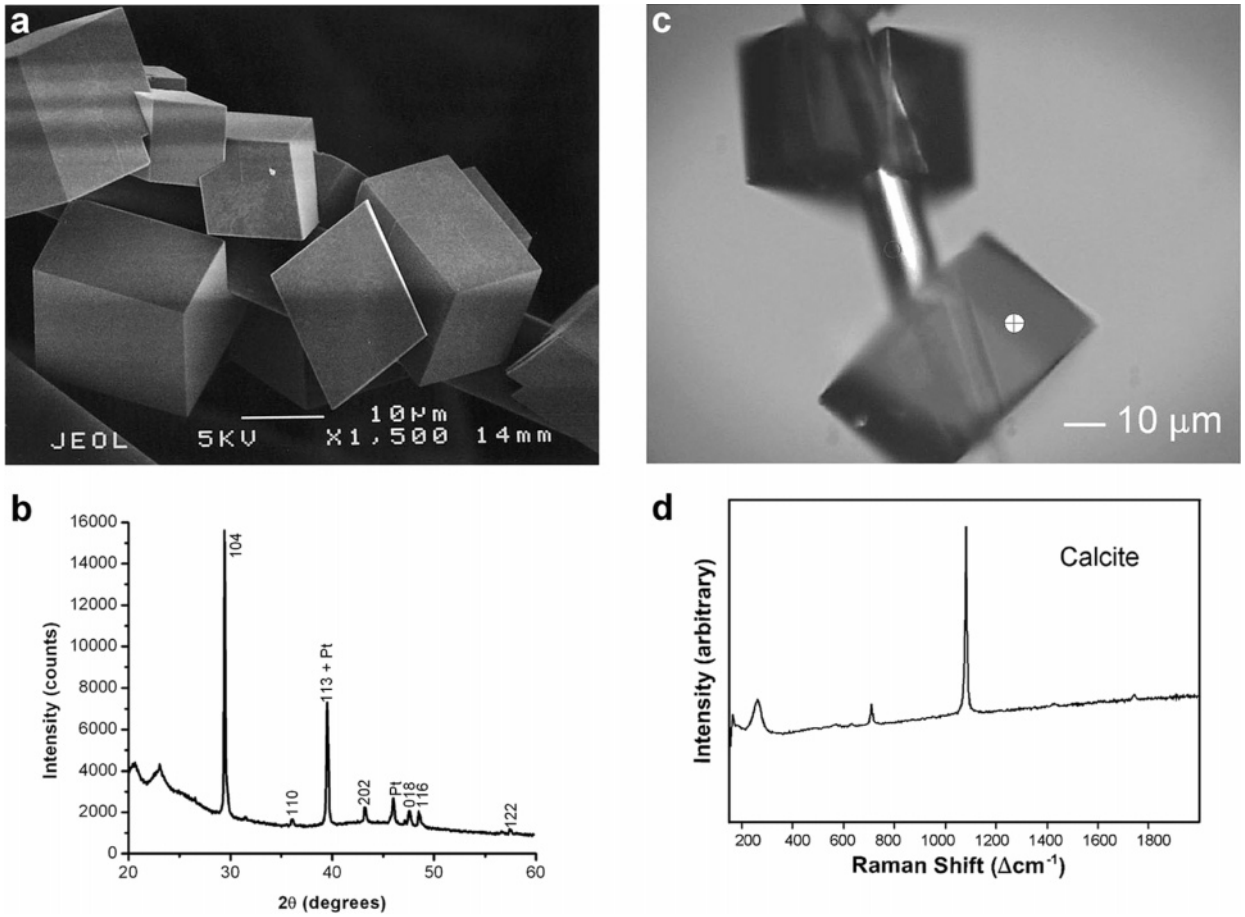

Figure 4. $CaCO_3$ crystals grown by slow diffusion on Kevlar fibers in the presence of control proteins. (a) SEM image of calcite rhombohedra grown for 3 days in the presence of 10 μg/mL calmodulin/S100 control proteins. Similar calcite rhombs also grew in the absence of any additives or in the presence of 10 μg/mL BSA. (b) X-ray diffraction pattern of rhombohedra contains only calcite peaks, including the dominant (104) peak. Background intensity from the platinum sample platform is labeled as (Pt). (c) Optical image and (d) Raman spectrum of an individual calcite crystal for polymorph determination. The exact position of the 1 μm area analyzed is indicated (○); characteristic Raman bands for calcite are at 280, 712, and 1086 Δcm^{-1}.

of the active AP8 protein concentration in solution (either by protein degradation and/or by occlusion within the crystals) led to the return of growth as calcite rhombohedra. It proved impractical to quantify accurately the amount of protein remaining in the crystallization solution, as the proteins must be recovered (i.e. repurified) in their entirety from the high salt-containing solution.

Polymorph Determination. Although the AP8-modified crystals morphologically resembled calcite rhombohedra, biogenic minerals can have morphologies vastly different from the low-energy equilibrium morphology dictated by the crystal lattice, presumably as a result of shape-modification by biomolecules.[2] Therefore, visual inspection of crystals grown in the presence of proteins is not sufficient to determine the polymorph. The polymorph of the AP8-modified crystals was thus determined by X-ray diffraction to be calcite at all time points; the example shown in Figure 6a is a calcite XRD pattern from crystals grown for 3 days with AP8. No significant differences in peak intensities were observed in the XRD patterns from AP8-modified calcite crystals when compared to those of unmodified calcite (Figure 4b). Furthermore, because calcite diffracts very intensely and may overwhelm the presence of any aragonite XRD peaks during analysis of the bulk sample, the micro-beam technique of Raman spectroscopy was used to confirm the calcite polymorph from micrometer-sized volumes of individual modified crystals (Figure 6b,c).

In another control experiment, we purposely initiated the growth of aragonite on Kevlar fiber substrates. In contrast to the effects observed by protein additives, the inclusion of PVA in the crystal growth solution at a concentration of 100 μg/mL induced the growth of a mixed population of calcite and aragonite crystals on Kevlar after 3 days of growth. Figure 7a is an SEM image of calcite rhombohedra and aragonite needle clusters positioned along a Kevlar fiber. The needle clusters are the macroscopic equilibrium morphology of aragonite grown in vitro. The presence of the aragonite polymorph was confirmed by XRD analysis of the bulk sample (Figure 7b), and by the detection of aragonite by Raman spectroscopic analyses of the individual needle clusters (Figure 7c,d). The reproducible nucleation of aragonite crystals on Kevlar fibers in the presence of PVA confirmed that biologically significant polymorphs could be grown under ambient conditions in this assay and led to the use of PVA as the "positive" control additive for aragonite polymorph selection.

Discussion

One of the challenges to a molecular understanding of $CaCO_3$ biomineralization is the purification of sufficient

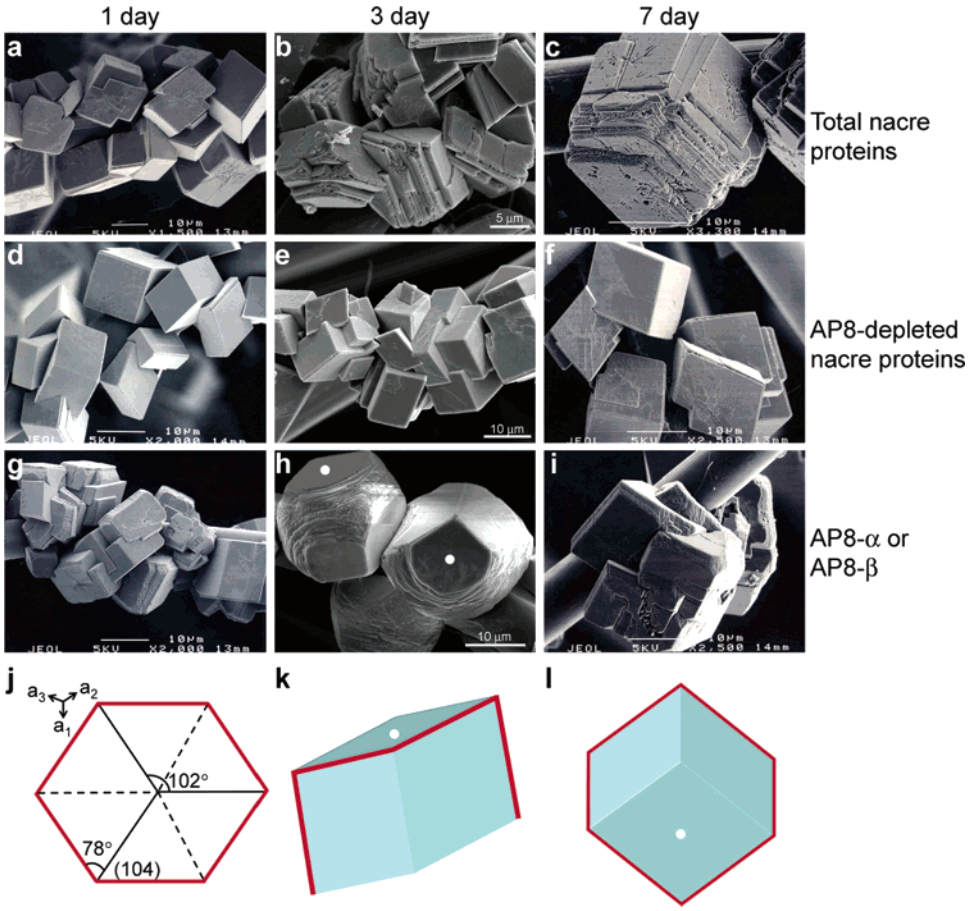

Figure 5. $CaCO_3$ crystals grown in the presence of different nacre protein fractions. SEM images of crystals nucleated and grown on Kevlar fibers in the presence of the total mixture of soluble nacre proteins (a−c), in the presence of nacre proteins that have been depleted of AP8 (d−f), and in the exclusive presence of either AP8-α or AP8-*β* protein (g−i). Crystals were grown with the proteins at a concentration of 10 *μ*g/mL over a period of 1 (a, d, g), 3 (b, e, h), or 7 (c, f, i) days. (j) A schematic calcite rhombohedron viewed down the *c*-axis. For each {104} face, the acute edges are labeled in red and the obtuse edges in black. The *a*-axes of the crystal are in the plane of the page as indicated; the *c*-axis projects perpendicular to the plane of the page through the intersections formed by three obtuse edges. (k−l) Three-dimensional models depicting the left (k) and right (l) crystals observed in the SEM image of 3-day AP8-modified calcite (h); corresponding faces between the observed and model crystals are indicated (○). The acute edges of the {104} faces are highlighted in red to show that they were specifically rounded by the AP8 proteins.

quantities of anionic proteins from mineralized composites for biochemical and functional characterization. This study describes two novel acidic proteins purified from abalone shell nacre. As the only proteins to remain soluble in a highly saturated solution of ammonium sulfate, the AP8 proteins were confirmed to be the most acidic ones from nacre by blue staining with Stains-All. Furthermore, the purification behavior and amino acid compositions of the AP8 proteins also demonstrate they are the most acidic proteins purified to date from biogenic aragonite.

The compositional similarities observed between the total mixture of nacre proteins and the AP8 proteins, including low hydrophobic content and the substantial presence of polar/charged and Gly residues, suggest that abalone nacre contains a collection of proteins with related functions that may depend on this biased amino acid composition. The AP8 proteins, however, stand out as the most significant contributors of Asx and Gly residues. In addition to putative AP8 cation binding by Asx residues, the presence of Lys and Arg residues may represent sites for interaction with the carbonate counterion. These acidic and basic residues, in conjunction with Ser and Glx residues, also may provide sites for hydrogen-bonding with water. The predominance of Gly, which represents nearly 40 mol % of the residues in the AP8 proteins, suggests considerable torsional flexibility along the protein backbone. This hypothesized structure will be evaluated in future studies to determine AP8 sequence and secondary structure.

HPLC purification of AP8 proteins from crystal-modulating contaminants rendered them suitable for in vitro mineralization assays. While the insoluble matrix in nacre contains a complex microlaminate of proteins, polysaccharides, and proteoglycans,[5,14,16,37,38] polyamide Kevlar fibers were selected to imitate this natural solid-phase crystal growth surface for in vitro mineralization. Other studies of soluble proteins extracted from shell have also used polymeric crystal growth substrates. The use of insoluble matrix sheets extracted from shells may be the most biologically relevant;[22,39,40] however, caveats to this approach stem from the lack of surface characterization and include complications such as the destruction of functional groups during the demineralizaton process and the persistence of small crystal nuclei. Alternatively, chemically simplified substrates composed of known components also have been employed,[20,23] and Kevlar fibers may be considered in this category of biomimetic crystal growth surfaces.

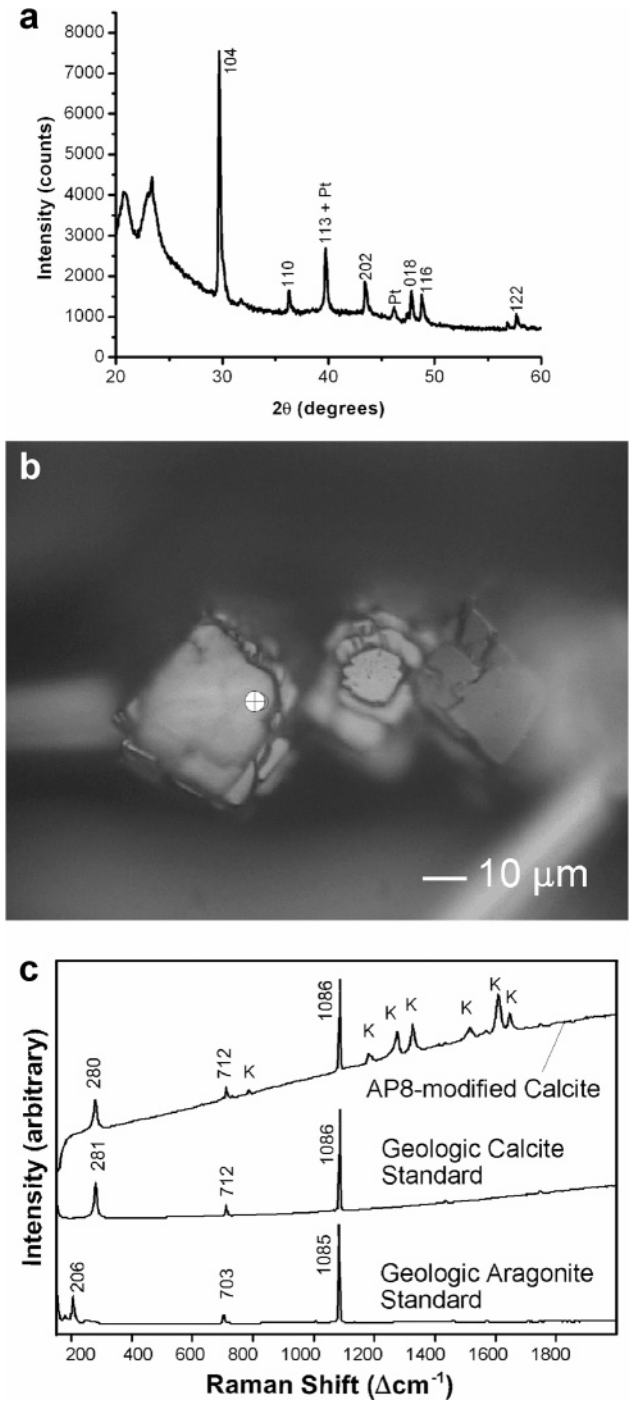

Figure 6. Polymorph determination of AP8-modified $CaCO_3$ crystals grown for 3 days. (a) X-ray diffraction pattern of the bulk sample contains only calcite peaks. (b) Optical micrograph of an individual AP8-modified crystal, showing characteristic rounding of two neighboring edges of the {104} face, analyzed in the 1 μm area (○) by Raman microprobe spectroscopy. (c) Raman spectra show that the AP8-modified crystals can unambiguously be identified as the calcite polymorph. Bands attributed to leakage from the Kevlar fiber during analysis of the crystals are indicated (K).

Using the Kevlar substrates, we present the first comparative study of crystal growth influenced by acidic biomineral-directing proteins both in isolation and in conjunction with other proteins. This approach thus allowed us to experimentally demonstrate that individual acidic proteins are stronger crystal-modulators than other proteins from the same biomineralized material. Specifically, the substantially diminished crystal-modulating activity observed by the AP8-depleted nacre proteins confirms that the acidic AP8 proteins are central to crystal growth control during mineralization. As expected from this result, the most pronounced effect on calcite morphology was induced by the purified AP8 proteins. Having confirmed that the polymorph of the AP8-modified crystals was calcite (Figure 6), it was discovered that the pair of rounded edges was identical for each crystal face, based on the geometry of the calcite crystal. Calcite rhombs have six parallelogram-shaped faces; each face is conjoined to two neighboring faces at an acute angle (78°) and two other faces at an obtuse angle (102°). Thus, acute and obtuse edges are defined as those that delineate respective acute and obtuse angles between rhomb faces. Figure 5j is a model of a rhombohedral calcite crystal with the acute edges shown in red and the obtuse edges in black for each of the (104) faces. The *a*-axes of the crystal are in the plane of the page, while the *c*-axis projects perpendicular to the plane of the page through the intersections formed by three obtuse edges. The depiction of calcite rhombs (Figure 5k,l), oriented to match respectively the left and right crystals shown in the SEM image of Figure 5h, clearly revealed that the acute edges (highlighted in red) of each of the (104) faces are rounded by the AP8 proteins after 3 days of growth. In contrast, the relative indifference of the AP8 proteins toward the obtuse edges is the only mechanism that would permit the retention of three straight intersecting edges from three separate {104} faces, as evidenced by the modified crystal on the right side of the SEM image in Figure 5h and drawn schematically in Figure 5l. The preferential interaction between AP8 proteins and the acute edges of rhomb faces indicates that these crystal surface locations are energetically and/or stereochemically favored by the proteins. In contrast, the effects of total nacre proteins were not as pronounced or as specific in their interactions with the acute edges of calcite faces as were the AP8 proteins. The crystals incubated with total protein have straighter edges, sharper corners, and larger macrosteps (Figure 5b) than crystals modified by the isolated AP8 proteins (Figure 5h). The lesser effect on crystal modification by the total nacre proteins at the acute edges mostly may reflect the greater relative concentration of AP8 proteins in the AP8-alone condition than in the total mixture. Other possible explanations for this observation, which are not mutually exclusive, include protein−protein interactions between AP8 and non-AP8 proteins, or nonspecific effects of non-AP8 proteins that interfere with the interaction between AP8 and the crystal surface.

The growth of calcite rhombohedra on Kevlar in the presence of control proteins demonstrates that crystal growth is relatively insensitive to nonspecific interactions. Of these proteins that have no known influence on biomineralization, BSA was chosen as a globular protein control, while the mixture of calmodulin and S100 proteins was chosen to represent small polyanionic proteins with known Ca^{2+} binding domains.[41] The absence of calcite modulation for crystals grown in the presence of the calmodulin/S100 proteins provided additional insights. The first is that the ability to sequester Ca^{2+} ions in solution at the concentration used for these anionic proteins was insufficient to perturb the most thermodynamically stable polymorph and morphol-

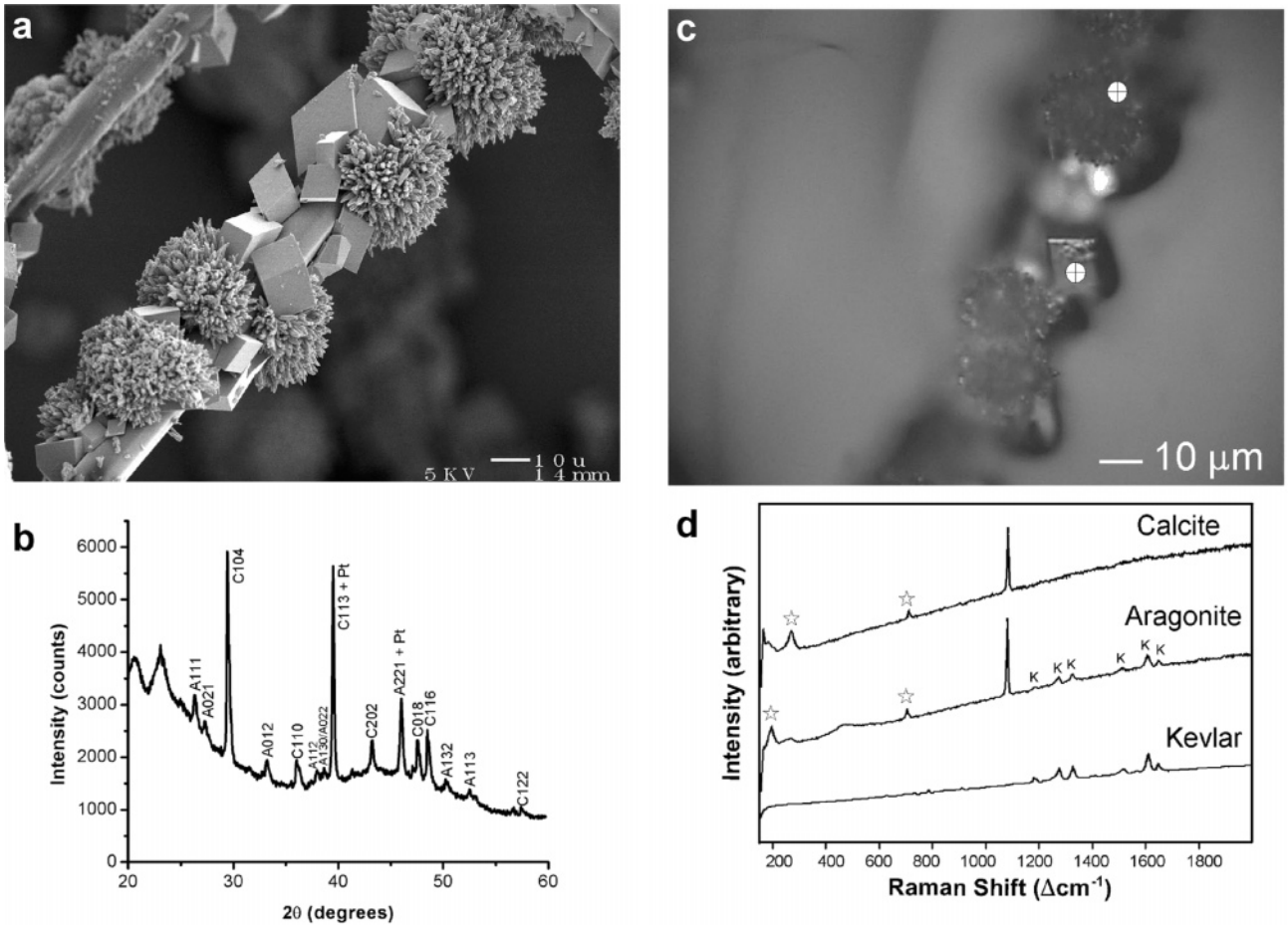

Figure 7. $CaCO_3$ crystals grown in the presence of poly(vinyl alcohol). (a) SEM image of calcite rhombohedra and aragonite needle clusters grown in the presence of 100 μg/mL PVA. (b) X-ray diffraction pattern of crystals grown with PVA contain both calcite (C) and aragonite (A) peaks. The intensity of the calcite (104) peak is reduced relative to baseline when aragonite is also present. (c) Optical image of individual crystals grown with PVA. The exact 1 μm sites of Raman microprobe laser interrogation are indicated (○). The top crystal is a needle cluster and the bottom crystal is a rhombohedron. (d) Needle cluster crystals produce the characteristic Raman bands for aragonite at 206, 703, and 1085 Δcm^{-1}, whereas rhombohedra produce the characteristic Raman bands for calcite at 280, 712, and 1086 Δcm^{-1}. The peak positions that differ distinctly between aragonite and calcite are marked (☆). Bands from the Kevlar substrate are indicated (K).

ogy of $CaCO_3$. A corollary of this interpretation is that the morphological modification of calcite achieved by the same concentration of the purified AP8 proteins involves precise interactions between the proteins and specific sites on the crystal surface. These interactions might occur between anions displayed by the proteins and sites of molecular complementarity on the crystal, as has been frequently suggested for a variety of related systems.[42−44]

The detection of aragonite on the Kevlar fibers in the presence of PVA confirmed previous studies showing that this fiber-adsorbed polymer can nucleate and sustain growth of this polymorph.[30] PVA displays a hydroxyl group in its repeating unit, which may be responsible for promoting adsorption to the Kevlar fiber and/or presenting sites that favor aragonite nucleation. This mechanism suggests that one possible reason aragonite was not formed on Kevlar in the presence of the nacre proteins may be the lack of sufficient hydroxyl-bearing Ser and Thr residues. Such a requirement for hydroxyl presentation may not exist in the natural system. In this respect, the Kevlar surface incompletely approximates the multicomponent insoluble matrix produced by the organism. It also is plausible that the AP8 proteins did not effectively interact with the Kevlar fibers (since only calcite was nucleated in the presence of these proteins), but instead have much higher affinity for specific locations on the mineral surface during crystallization. This suggestion is strongly supported by the observed asymmetric crystal morphology in which only acute edges were affected by AP8. Histological examination of nacre cross sections probed with anti-AP8 antibodies may reveal whether AP8 is localized on the insoluble matrix or embedded within individual crystals.

The mechanism of polymorph selection in mollusk shells remains unclear. In the shell of many species, the outer calcite layer directly abuts the inner aragonite layer. In this region of the abalone shell, the needle-shaped calcite crystals even penetrate into the aragonite tablets, indicating there is no defined organic boundary between the different polymorphs.[3] This abrupt polymorph transition suggests that some proteins may act to inhibit calcite formation, possibly by decreasing calcite solubility or altering the calcite surface in preparation for aragonite overgrowth. This type of activity may be initiated by the acidic AP8 proteins through their observed strong affinity for specific regions of the calcite surface.

The fact that the nacre proteins did not promote aragonite crystallization in our experiments may reflect the lack of some essential components such as Mg^{2+} ions or the chemical and physical microenvironment provided by the

insoluble protein matrix normally required for aragonite polymorph formation. It is now our hope that definition of the sites of interaction of the nacre proteins with the atomic lattice of calcite through experiments such as we report here may help identify the specific lattice planes of aragonite that are stabilized by these proteins in vivo. The relevance of the current findings to the process of shell construction in the living organism therefore remains to be determined.

The successful purification of the AP8 proteins provides a reagent with which to begin investigating the molecular determinants that underlie the functional importance of highly acidic proteins during $CaCO_3$ mineralization. Although sequencing of peptides derived from the digested AP8 proteins has been hindered by overly strong peptide binding to Edman sequencing membranes and by ESI-MS/MS peptide fragmentation patterns rendered uninterpretable by repetitive sequence motifs (G. Fu and D. E. Morse, unpublished observations), future efforts will deduce amino acid sequences from the cloned cDNAs. Since the activity of the AP8 proteins appears to be primarily at the surface of growing crystals, structural analyses of the proteins' "ligand" (i.e., the modified crystal surface) also is merited. Molecular imaging of AP8-modified calcite by AFM has been recently undertaken (G. Fu, S. R. Qiu, D. E. Morse, and J. J. De Yoreo, in preparation) to identify the mechanism of protein−mineral interaction at the acute edges of growing calcite.[45] Thus future studies building on the initial structural analyses presented here of both the acidic AP8 proteins and the $CaCO_3$ crystals they modify ultimately will lead to a description of molecular recognition that may be compared to the mechanisms that are emerging for the more established calcium phosphate biomineral systems.[42,43,46]

Acknowledgment. This work was supported by grants from the UC Systemwide Biotechnology Research and Education Program through grant UC Biotechnology/2001-16; the NASA University Research, Engineering and Technology Institute on Bio Inspired Materials (BIMat), under award No. NCC-1-02037; the Institute for Collaborative Biotechnologies, through grant DAAD19-03-D-0004 from the U.S. Army Research Office; and the MRSEC Program of the National Science Foundation, under award No. DMR-96-32716 to the UCSB Materials Research Laboratory. One of the authors (B. W.) was supported by the U.S. National Science Foundation under Grant No. 0210247.

References and Notes

(1) Lowenstam, H. A. *Science* **1981**, *211*, 1126−1131.
(2) Mann, S. *Biomineralization: Principles and concepts in bioinorganic materials chemistry*; Oxford University Press: Oxford, 2001.
(3) Zaremba, C. M.; Belcher, A. M.; Fritz, M.; Li, Y.; Mann, S.; Hansma, P. K.; Morse, D. E.; Speck, J. S.; Stucky, G. D. *Chem. Mater.* **1996**, *8*, 679−690.
(4) Su, X.; Belcher, A. M.; Zaremba, C. M.; Morse, D. E.; Stucky, G. D.; Heuer, A. H. *Chem. Mater.* **2002**, *14*, 3106−3117.
(5) Nakahara, H. In *Mechanisms and phylogeny of mineralization in biological systems*; Suga, S., Nakahara, H., Eds.; Springer-Verlag: Tokyo, 1991; pp 343−350.
(6) Mutvei, H. In *Origin, evolution and modern aspects of biomineralization in plants and animals*; Crick, R. E., Ed.; Plenum Press: New York, 1989; pp 137−151.
(7) Currey, J. D. *Proc. R. Soc. London Ser. B: Biol. Sci.* **1977**, *196*, 443−463.
(8) Tang, Z.; Kotov, N. A.; Magonov, S.; Ozturk, B. *Nat. Mater.* **2003**, *2*, 413−418.
(9) Sellinger, A.; Weiss, P. M.; Nguyen, A.; Lu, Y.; Assink, R. A.; Gong, W.; Brinker, C. J. *Nature* **1998**, *394*, 256−260.
(10) Weiner, S.; Addadi, L. *Trends Biochem. Sci.* **1991**, *16*, 252−256.
(11) Marsh, M. E. *Bull. Inst. Oceanogr. Monaco* **1994**, *14*, 121−128.
(12) Addadi, L.; Weiner, S. *Angew. Chem.* **1992**, *104*, 159−176.
(13) Michenfelder, M.; Fu, G.; Lawrence, C.; Weaver, J. C.; Wustman, B. A.; Taranto, L.; Evans, J. S.; Morse, D. E. *Biopolymers* **2002**, *70*, 522−533.
(14) Shen, X.; Belcher, A. M.; Hansma, P. K.; Stucky, G. D.; Morse, D. E. *J. Biol. Chem.* **1997**, *272*, 32472−32481.
(15) Miyashita, T.; Takagi, R.; Okushima, M.; Nakano, S.; Miyamoto, H.; Nishikawa, E.; Matsushiro, A. *Mar. Biotechnol.* **2000**, *2*, 409−418.
(16) Sudo, S.; Fujikawa, T.; Nagakura, T.; Ohkubo, T.; Sakaguchi, K.; Tanaka, M.; Nakashima, K.; Takahashi, T. *Nature* **1997**, *387*, 563−564.
(17) Marin, F.; de Groot, K.; Westbroek, P. *Protein Express. Purif.* **2003**, *30*, 246−252.
(18) Sarashina, I.; Endo, K. *Mar. Biotechnol.* **2001**, *3*, 363−369.
(19) Tsukamoto, D.; Sarashina, I.; Endo, K. *Biochem. Biophys. Res. Commun.* **2004**, *320*, 1175−1180.
(20) Gotliv, B.-A.; Addadi, L.; Weiner, S. *ChemBioChem* **2003**, *4*, 522−529.
(21) Aizenberg, J.; Lambert, G.; Weiner, S.; Addadi, L. *J. Am. Chem. Soc.* **2002**, *124*, 32−39.
(22) Belcher, A. M.; Wu, X. H.; Christensen, R. J.; Hansma, P. K.; Stucky, G. D.; Morse, D. E. *Nature* **1996**, *381*, 56−58.
(23) Falini, G.; Albeck, S.; Weiner, S.; Addadi, L. *Science* **1996**, *271*, 67−69.
(24) Berman, A.; Addadi, L.; Weiner, S. *Nature* **1988**, *331*, 546−548.
(25) Albeck, S.; Aizenberg, J.; Addadi, L.; Weiner, S. *J. Am. Chem. Soc.* **1993**, *115*, 11691−11697.
(26) Feng, Q. L.; Pu, G.; Pei, Y.; Cui, F. Z.; Li, H. D.; Kim, T. N. *J. Cryst. Growth* **2000**, *216*, 459−465.
(27) Suzuki, M.; Murayama, E.; Inoue, H.; Ozaki, N.; Tohse, H.; Kogure, T.; Nagasawa, H. *Biochem. J.* **2004**, *382*, 205−213.
(28) Wilt, F. H.; Killian, C. E.; Livingston, B. T. *Differentiation* **2003**, *71*, 237−250.
(29) Waite, J. H. *Anal. Biochem.* **1991**, *192*, 429−433.
(30) Lakshminarayanan, R.; Valiyaveettil, S.; Loy, G. L. *Cryst. Growth Des.* **2003**, *3*, 953−958.
(31) Campbell, K. P.; MacLennan, D. H.; Jorgensen, A. O. *J. Biol. Chem.* **1983**, *258*, 11267−11273.
(32) Cariolou, M. A.; Morse, D. *J. Comp. Physiol. B* **1988**, *157*, 717−729.
(33) Miyamoto, H.; Miyashita, T.; Okushima, M.; Nakano, S.; Morita, T.; Matsushiro, A. *Proc. Natl. Acad. Sci. U.S.A.* **1996**, *93*, 9657−9660.
(34) McGrath, K. P.; Fournier, M. J.; Mason, T. L.; Tirrell, D. A. *J. Am. Chem. Soc.* **1992**, *114*, 727−733.
(35) Addadi, L.; Moradian, J.; Shay, E.; Maroudas, N. G.; Weiner, S. *Proc. Natl. Acad. Sci. U.S.A.* **1987**, *84*, 2732−2736.
(36) Addadi, L.; Weiner, S. *Proc. Natl. Acad. Sci. U.S.A.* **1985**, *82*, 4110−4114.
(37) Weiss, I. M.; Renner, C.; Strigl, M. G.; Fritz, M. *Chem. Mater.* **2002**, *14*, 3252−3259.
(38) Weiner, S.; Traub, W. *FEBS Lett.* **1980**, *111*, 311−316.
(39) Kono, M.; Hayashi, N.; Samata, T. *Biochem. Biophys. Res. Commun.* **2000**, *269*, 213-218.
(40) Samata, T.; Hayashi, N.; Kono, M.; Hasegawa, K.; Horita, C.; Akera, S. *FEBS Lett.* **1999**, *462*, 225−229.
(41) Heizmann, C. W.; Cox, J. A. *BioMetals* **1998**, *11*, 383−397.
(42) Hoang, Q. Q.; Sicheri, F.; Howard, A. J.; Yang, D. S. C. *Nature* **2003**, *425*, 977−980.
(43) Long, J. R.; Shaw, W. J.; Stayton, P. S.; Drobny, G. P. *Biochemistry* **2001**, *40*, 15451−15455.
(44) Weiner, S.; Hood, L. *Science* **1975**, *190*, 987−989.
(45) Teng, H. H.; Dove, P. M.; Orme, C. A.; DeYoreo, J. J. *Science* **1998**, *282*, 724−727.
(46) He, G.; Dahl, T.; Veis, A.; George, A. *Nat. Mater.* **2003**, *2*, 552−558.

BM049314V